Estimating the Masses and Centers of Mass of Extinct Animals by 3-D Mathematical Slicing

Donald M. Henderson

Paleobiology, Vol. 25, No. 1 (Winter, 1999), 88-106.

Stable URL:
http://links.jstor.org/sici?sici=0094-8373%28199924%2925%3A1%3C88%3AETMACO%3E2.0.CO%3B2-N

Paleobiology is currently published by Paleontological Society.

Paleobiology, 25(1), 1999, pp. 88–106

Estimating the masses and centers of mass of extinct animals by 3-D mathematical slicing

Donald M. Henderson

Abstract.—A mathematical-computational method for determining the volume, mass, and center of mass of any bilaterally symmetric organism is presented. Cavities within the body of an organism such as lungs are easily accommodated by this method. Sagittal and frontal profiles, obtained from tracings of "fleshed-out" skeletal reconstructions, are used to provide limits for defining transverse slices of the body. Any internal cavities are defined by their own sagittal and frontal profiles. The computations consist of mathematically slicing the body and any cavities into independent sets of transverse laminae and computing their masses, centroids, and moments with respect to the three coordinate axes. Further calculations produce the masses and the (x,y,z) coordinates for the centers of mass of the body, any cavities, and the body + cavities. Predicted body masses of large, extant mammals (elephant, giraffe, hippopotamus, and rhinoceros) are in close agreement with actual body masses. New, lower estimates for body masses of selected large dinosaurs, based on modern skeletal reconstructions, are also presented, along with numerical estimates of their centers of mass. This method is an improvement over earlier ones that relied on measuring displaced volumes of water or sand by scale models to estimate the masses, and suspending models by threads to estimate their centers of mass.

Donald M. Henderson. Department of Earth Sciences, University of Bristol, Bristol BS8 1RG United Kingdom

Accepted: 3 August 1998

Introduction

Zoologists and paleontologists are interested in knowing the ecological roles of the organisms that they study. Zoologists have the luxury of observing their organisms directly, while paleontologists have to find proxies for inferring the habits of their long-extinct organisms. The adult body mass of an animal determines, in large part, its ecological role, and there is a large literature on the subject (see Damuth and MacFadden 1990, and references therein, for a comprehensive review). Estimating the mass of an extinct animal will give insights into how that animal functioned as a living organism.

For biomechanical studies a simple scalar body mass is of limited use. It says nothing about how a three-dimensional collection of muscles, bones, skin, and organs, being pulled by gravity, pushed by moving air, or buoyed up by water, reacts in a three-dimensional world. Knowing the distribution of the body mass of an organism extends our knowledge from one dimension into the much richer, three-dimensional world of forces, levers, torques, and balance. The center of mass of an animal conveniently summarizes the distribution of body mass and simplifies analysis. The position of the center of mass of an organism has important implications in both stable equilibrium situations such as standing on two legs (Weishampel 1995), and unstable equilibrium situations such as walking and running (Gatesy and Biewener 1991) and flying (Bramwell and Whitfield 1974). Having an estimate of the center of mass of an extinct animal, combining it with inferred muscle and bone mechanics and, in the case of terrestrial tetrapods, trackway data, allows for a more complete picture of how an extinct animal could have moved and what it would have been capable of.

One set of methods for determining the mass of an extinct animal is based on estimating the volume of the animal. A life reconstruction is produced to provide a volume estimate, and an assumption of the bulk density of the body tissues is made. The product of this assumed density and the body volume gives an estimate of the mass. Colbert (1962) presented an updated form of this method, which was first used by W. K. Gregory (1905)

 0094-8373/99/2501-0006/$1.00

to estimate the masses of large dinosaurs. Both Colbert and Gregory used scale models and estimated the volumes of their models by measuring the displacement of some "fluid" by their models. Gregory used water as his displacement material, while Colbert used dry sand. Neither Gregory nor Colbert looked at how the masses of their models were distributed; they simply measured the displacements of whole models to get bulk mass estimates.

An important paper analyzing the magnitudes and distributions of body masses of extinct vertebrates was published by R. McNeil Alexander (1985). His method also relied on measuring the amounts of water displaced by scale models, but Alexander's method improved on the one outlined by Colbert. Alexander viewed his models as being a sequence of thick slices, and measured the volumes of these body slices by incrementally immersing the models in water and recording the volume of fluid displaced by a slice and its axial position. Combining the volume data with the position data and converting the volumes to masses allowed Alexander to calculate not only the total body mass, but also the distribution of body mass. Noting that the center of mass (CM) can be expected to lie somewhere in the sagittal plane between the limb girdles, Alexander visually estimated the position of the CM while the model was suspended vertically, in several orientations, and allowed to reach its equilibrium position (method outlined in Alexander 1983). Unlike Colbert, Alexander took into account the effect of the lungs on the position of the CM. Lungs represent an asymmetrically distributed region of lower density that will have a small, but measurable, effect on an animal's CM and mass.

This paper presents a method to compute the volume (mass) of an animal, and extends the methods of Alexander in order to locate precisely the CM in three-dimensional space. Instead of working with a physical three-dimensional model, the method works with a mathematical one. It uses a computer to subdivide an abstract, mathematical volume and perform the tedious calculations necessary to compute and sum the volumes and moments of many smaller subvolumes. Once the initial data have been collected, this numerical method provides estimates of mass and the CM quickly and easily. Although the focus of this paper is on vertebrates, the method outlined here can be applied to any bilaterally symmetric organism.

It should be noted that the numerical slicing and weighing technique presented here was anticipated in a simpler form by Bramwell and Whitfield (1974). The present method is a more mathematically sophisticated one that overcomes several of the simplifying assumptions that Bramwell and Whitfield had to make and permits a more detailed analysis of mass distribution.

Method

Data Collection

The first stage is the collection of the sagittal and frontal profile data, which come from outline drawings of lateral and dorsal views of a skeletal reconstruction with the flesh outlines (muscles and skin) included. The dorsal and ventral, and left and right profile lines will be treated as lines in two-dimensional coordinate space. The x-axis is parallel to, or co-axial with, the dorsal segments of the spinal column. The axis perpendicular to the x-axis, the y, will represent the dorso-ventral dimension. Perpendicular to the plane defined by the x and y axes is the z-axis. Positive and negative z-values refer to the right and left sides of the body respectively.

Lines are drawn across both profiles such that each line will cross top and bottom, or left and right, edges of the outlines. Figure 1 shows the pattern of lines drawn across the lateral and frontal profiles of *Tyrannosaurus rex* (modified from Paul 1988: p. 341). The intersections of the straight lines with the profile edges define points, and these points can be used to define an edge as a series of connected points ("connect-the-dots").

The sagittal profile lies in the xy plane, and the intersections of the straight lines with this profile gives a series of (x,y) pairs. Profile segments that are strongly curved relative to other segments will require more points of intersection in order to record the form of the curve

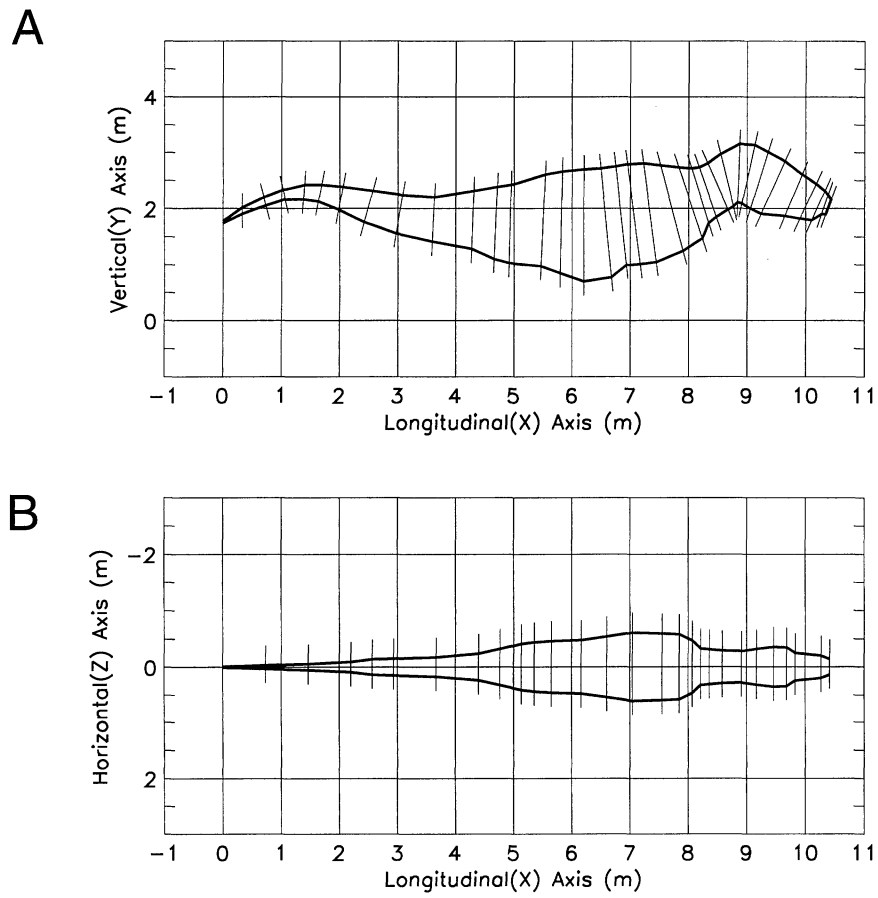

FIGURE 1. Lateral (A) and frontal (B) profiles of *Tyrannosaurus rex* (after Paul 1988: p. 341) with slice traces overlying the body outlines. The points of intersection of the slices with the profiles provide sets of coordinates in the xy and xz planes. Combining the xy and xz data produces a series of ellipses that are three-dimensional, transverse slices of the body.

more precisely than segments that are less curved. The head and neck will usually require relatively closely spaced lines, while the caudal regions can be sampled quite coarsely. However, it was found that body forms generated from tracings with a more uniform spacing between the slices looked much better.

The frontal profile lies in the x-z plane, and lines that traverse this profile provide a series of (x,z) pairs that give the dimensions of the right and left sides of the body. Even though vertebrates are bilaterally symmetric, reconstructions are often slightly unbalanced. Recording both left and right dimensions, and then averaging them, smooths out any unevenness in the reconstructions.

The best method to capture the numerical values for the sets of coordinates defining profiles is to use a digitizing tablet in conjunction with a computer aided drafting package (CAD) such as AutoCAD or paint program like Canvas. With the profile drawings positioned on the digitizing tablet, the stylus of the tablet is used to touch the body profiles where they are crossed by transverse lines. Programs like AutoCAD or Canvas can record the vertical and horizontal coordinates returned by the digitizing tablet and write the sets of coordinate points as files for later use. The coordinate values can be converted to full-scale values by multiplying them by the scale used in the original figure.

An alternative way to get the point coordinates is to trace the outline drawings onto graph paper with the animal's long dimension aligned with one of the graph paper axes. Nu-

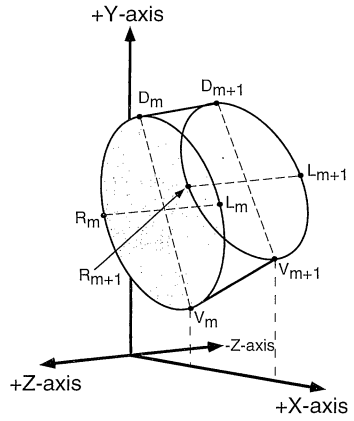

FIGURE 2. Configuration of a hypothetical m^{th} body slab, possibly from a cervical segment. The ends are defined by the m^{th} and $(m + 1)^{th}$ tranverse slices. D_m, V_m, L_m, and R_m are dorsal, ventral, left, and right points respectively of the m^{th} slice.

merical values for the intersection points can be determined from the graph paper axes, and the numbers can be typed into a simple text editing program to produce data files for later use.

Data Organization

The sagittal xy-intercept data and the frontal xz-intercept data are used to define the semi-major and semi-minor radii of a series of ellipses that represent a set of transverse slices across the body. The bodies of most vertebrates are deeper than they are wide, and the semi-major axis is considered to be this deeper sagittal depth. Half the distance between the dorsal and ventral intercepts of a slice provides a value for the semi-major radius. The narrower left-right dimension is considered to be the semi-minor axis, and the semi-minor radius is half the distance between the right and left intercept values. The semi-minor axis intercepts the semi-major axis at the midpoint of the line joining the dorsal and ventral intercepts.

This set of transverse slices can be used to divide the body into a series of slabs with elliptical cross sections and parallel or subparallel ends. These slabs are defined by pairs of adjacent elliptical slices. Figure 2 illustrates the configuration of a hypothetical slab formed from the m^{th} and $(m + 1)^{th}$ slices. Figure 3 shows the transverse slice data for the *Tyrannosaurus,* measured in Figure 1, transformed into a three-dimensional body form. This body form is a hollow "mesh" of rectangular polygons. The vertices of the polygons are points defining the edges of the slices. These points have been inserted with a constant angular spacing and lie in the plane of each slice.

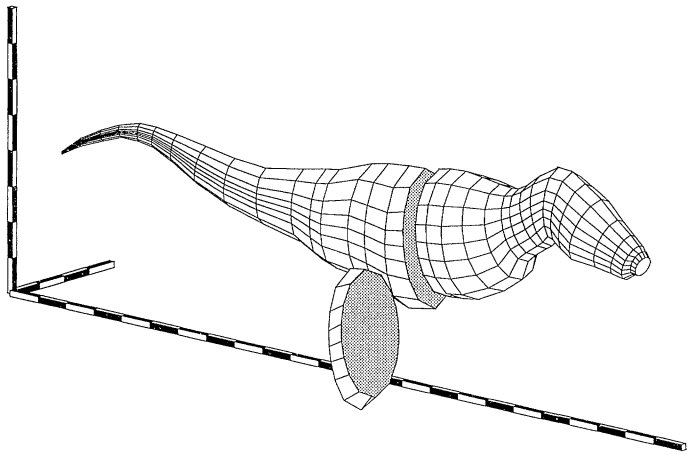

FIGURE 3. Three-dimensional reconstructed body form of *Tyrannosaurus rex* derived by mathematically combining and extending the two sets of 2-D data recorded from Figure 1. A representative body slab has been drawn out to show that the body form can be viewed as a collection of independent disk-like units. This body form is actually a hollow, elliptical shell, and the darker color of the cut surfaces is purely an illustrative aid. The longitudinal axis is 12 m long, the vertical axis is 4 m, and the short transverse axis is 2 m. Increments on all the scale bars are 50 cm.

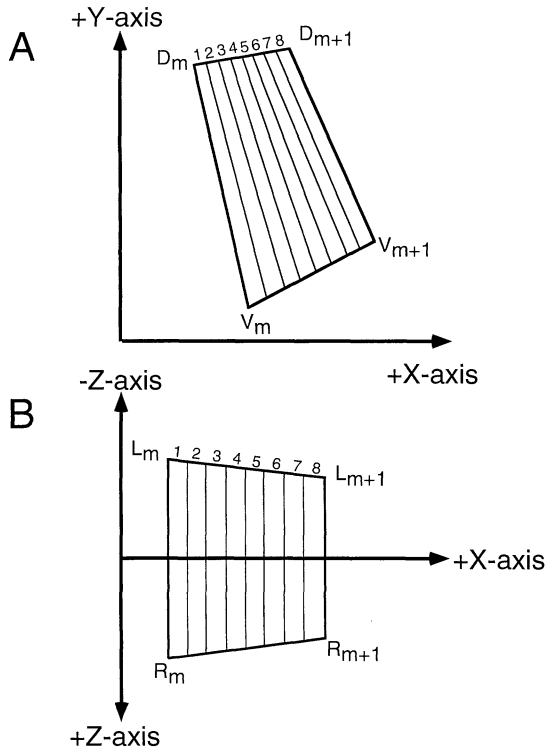

FIGURE 4. Sagittal (A) and frontal (B) views of the subdivisions of the m^{th} slab of Figure 2 to produce subslabs for use in computing mass and center of mass of the slab.

Computations

Slab and Subslab Geometry.—The spatial resolution afforded by the body slabs is too coarse for computations of body volumes and dynamical properties. Precise determination of the centroids and moments with respect to the three coordinate axes requires that the slabs be subdivided into thinner subslices. The dorsal, ventral, left, and right dimensions of these subslices are formed by computing seven intermediate points between major points to give eight subslabs. This subslicing is shown in Figure 4. The x-axis and y-axis separations of the dorsal points of the m^{th} and $(m + 1)^{th}$ slices would be specified as follows:

$$\begin{bmatrix}\Delta D_x\\ \Delta D_y\end{bmatrix}_m = \frac{1}{N-1}\left(\begin{bmatrix}D_x\\ D_y\end{bmatrix}_{m+1} - \begin{bmatrix}D_x\\ D_y\end{bmatrix}_m\right) \quad (1)$$

where D_x and D_y are the dorsal x- and y-axis coordinates and N is the number of required subslices of the m^{th} slab ($N = 8$ in the present example). The position of the dorsal point of n^{th} subslab would be then given by

$$\begin{bmatrix}d_x\\ d_y\end{bmatrix}_n = \left(n + \frac{1}{2}\right)\begin{bmatrix}\Delta D_x\\ \Delta D_y\end{bmatrix}_m + \begin{bmatrix}D_x\\ D_y\end{bmatrix}_m \quad (2)$$

and n takes on the values from 0 to $N - 1$. The 1/2 term shifts the x and y positions to the midpoint of the subslab. Similar expressions are used to interpolate intermediate points for the ventral, left, and right edges of slabslabs.

Center points are determined for each subslice by treating the dorsal, ventral, left, and right limits of a subslice as coordinates in three-dimensional space. The vector form of the midpoint formula is then used to compute the centers of each slice using the dorsal and ventral points. The center of the n^{th} subslice is expressed as follows:

$$\begin{bmatrix}c_x\\ c_y\\ c_z\end{bmatrix}_n = \frac{1}{2}\left(\begin{bmatrix}d_x\\ d_y\\ d_z\end{bmatrix}_n + \begin{bmatrix}v_x\\ v_y\\ v_z\end{bmatrix}_n\right) \quad (3)$$

where c_n, d_n, and v_n are the coordinate triples for the center, dorsal, and ventral points respectively. The bilateral symmetry of vertebrates leads to the z-term of the dorsal, center, and ventral points being equal to zero, but for later computations involving transverse quantities it is necessary to carry the z-term.

These later computations require the semi-major and semi-minor radii of subslices to be treated as vectors in three-dimensional space. These radial vectors can be derived by vector subtraction of the center point of a subslice from the dorsal and lefthand side points of the subslice:

$$\begin{bmatrix}RR_x\\ RR_y\\ RR_z\end{bmatrix}_n = \begin{bmatrix}d_x\\ d_y\\ d_z\end{bmatrix}_n - \begin{bmatrix}c_x\\ c_y\\ c_z\end{bmatrix}_n$$

$$\begin{bmatrix}rr_x\\ rr_y\\ rr_z\end{bmatrix}_n = \begin{bmatrix}l_x\\ l_y\\ l_z\end{bmatrix}_n - \begin{bmatrix}c_x\\ c_y\\ c_z\end{bmatrix}_n \quad (4)$$

where RR_n and rr_n are the semi-major and semi-minor radii vectors respectively of the n^{th} subslice, and c_n, d_n, and l_n are the center, dorsal, and left points respectively. With the two radii of a subslice in vector form it is now

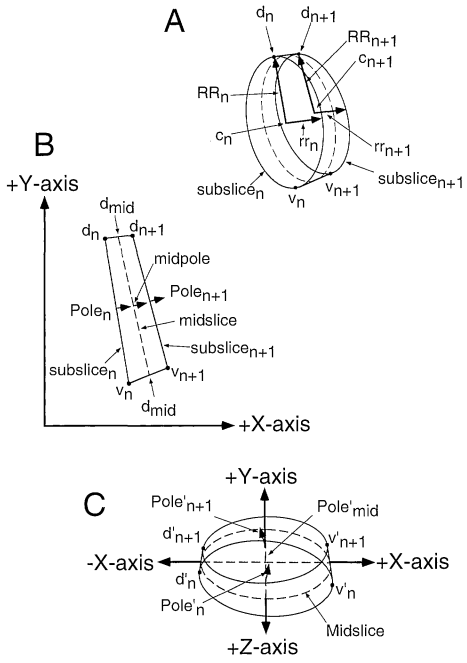

FIGURE 5. A, Lateral, oblique view of the n^{th} subslab showing the vector representation of the semi-major, RR_n and RR_{n+1}, and semi-minor, rr_n and rr_{n+1}, radii of the n^{th} and $(n + 1)^{th}$ subslices that bound the n^{th} subslab. The center points of the subslices are represented by c_n and c_{n+1}. The dashed ring indicates the position of the midslice between the two bounding slices. B, Sagittal view of the n^{th} subslab showing the positions and directions of points and vectors in the xy plane prior to rotation. The poles to the subslices, $Pole_n$ and $Pole_{n+1}$ are derived by computing the vector products of the semi-minor and semi-major radii of a subslice. C, Dorsal, oblique view of the n^{th} subslab after counterclockwise rotation to align the midslice pole with the y-axis, and shifting the subslab to have it centered on the origin. The n^{th} and $(n + 1)^{th}$ subslices now form the lower and upper surfaces respectively of an elliptical cylinder, while the lateral surface of this cylinder intersects the xz plane along the line defined by the perimeter of midslice. Primed (') quantities denote the rotated and translated quatities from B.

possible to represent each subslice as a plane in three dimensions. This is most concisely done by determining a pole perpendicular to the plane. This pole is simply the vector cross-product of the semi-major and semi-minor radii vectors:

$$P_n = rr_n \times RR_n \quad (5)$$

This geometry for a hypothetical subslab is shown in Figure 5A.

Volume Calculations.—Knowing the center points of the subslices and the poles to the planes that contain the subslices will allow the derivation of simple linear equations that can be used to mathematically describe the planes. With the equations of the planes (subslices) known it is possible to compute the volumes of subslabs bounded by consecutive pairs of subslices.

The varying orientation of adjacent slices relative to one another, and the fact that slices will rarely be parallel to the yz-plane, make the computations complicated, but this complexity can be reduced by reorienting the subslices that bound subslabs. The method used here determines the center and perpendicular pole to a plane that is midway between two bounding planes. Definition of this midplane, in lateral view, is seen in Figure 5B. The midplane pole, and the poles of the associated bounding planes, are then rotated counterclockwise until the midplane pole is aligned with the y-axis. The centers of all three planes are then translated until the midplane center is at the origin of the coordinate system. In addition to rotating the poles and translating the centers of the three slices, their associated dorsal, ventral, and lateral points are rotated and translated as well. The effects of these rotations and translations on the two bounding subslices and their mutual midslice are shown in Figure 5C. The midslice now lies in the xz plane, centered on the origin, and the subslice with the low subscript, n, is below the midplane, while the subslice with the higher subscript, $n + 1$, lies above the midplane. The dorsal points of all three slices have been repositioned to lie on, or perpendicular to, the negative x-axis, while their ventral points now lie in the region around the positive x-axis. The lower and upper slices form the bottom and top bounding surfaces of a cylinder with elliptical cross section.

The volume of the n^{th} subslab can be computed by evaluating a double integral over the elliptical region, R, defined by the perimeter of the midplane slice in the xz plane:

$$volume_n = \int\int_R \{f_{top}(x, z) - f_{bottom}(x, z)\}\, dx\, dz \quad (6)$$

where $f_{bottom}(x,z)$ and $f_{top}(x,z)$ are the equations

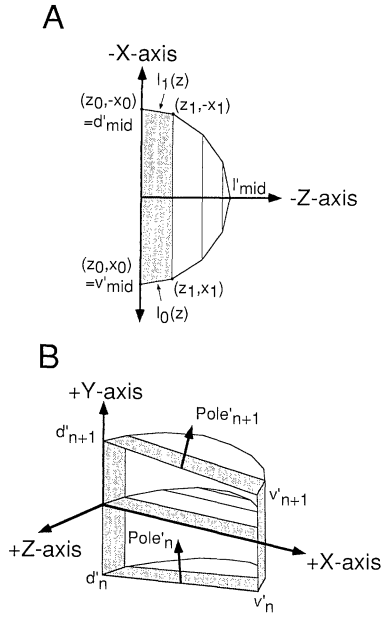

FIGURE 6. A, Plan view of the left side of the midslice in the xz plane. The first trapezoidal subregion of the midslice is colored gray. Linear functions l_0 and l_1 describe the upper and lower bounds of the trapezoid as functions of z. B, Oblique view of the subvolume associated with the region of integration defined in part A.

of the bottom and top bounding planes respectively and have the form

$$f(x,z) = c + ax + bz \tag{7}$$

where c, a, and b are coefficients determined from the pole and center of the each subslice using standard methods from linear algebra that relate vectors and points in planes (O'Neil 1983: pp. 594–599).

The vertices that were generated to define the perimeter points of the model slices provide a convenient set of points for use in subdividing the midslice into trapezoidal subregions to allow the integration to be performed. The subdivisions of the left-hand side of the midslice are shown in Figure 6A, and the volume defined by the bounding planes and the first trapezoidal region are shown in Figure 6B. The integral to compute this volume is

$$trap\_volume = \int_{z=z_0}^{z_1} \int_{x=l_0(z)}^{l_1(z)} \{f_{top}(x, z) - f_{bottom}(x, z)\}\, dx\, dz \tag{8}$$

where $l_0(z)$ and $l_1(z)$ are equations of the form $l(z) = mz + b$ that describe the upper and lower boundaries of the trapezoidal region of integration. Bilateral symmetry means that only the volumes defined by trapezoidal subregions on one side of the sagittal plane of a subslab need to be done by integration, and doubling the sum of their volumes gives the total volume n^{th} subslab:

$$subslab\_volume_n = 2 \sum_{t=0}^{V/4-1} trap\_volume_t \tag{9}$$

where V is the number of vertices, a multiple of 4, used to define the midslice perimeter. The volume of the m^{th} slab is just the sum of the volumes of the N subslabs:

$$slab\_volume_m = \sum_{n=0}^{N-1} subslab\_volume_n \tag{10}$$

The total volume of the body defined by the sum of the slabs:

$$body\_volume = \sum_{m=0}^{M-1} slab\_volume_m \tag{11}$$

where M is the number of slices that the body mesh was initial defined with.

Center of Mass Calculations.—To determine the center of mass (CM) of a subslab it is only necessary to determine the centroid of the quadrilateral defined by the sagittal profile of the subslab, and to convert this centroid into a CM by multiplying it by the mass of the subslab. The bilateral symmetry of vertebrates means that the CM has no lateral component and lies completely within this sagittal plane.

The first step to compute the centroid (Cd) is to get the area of the region. This can be done quickly and simply by breaking the region into three smaller subregions: a top triangle, a middle, rectangular region, and a bottom triangle. These subregions of the sagittal quadrilateral are shown in Figure 7. The top and bottom sides of the quadrilateral can be expressed as simple linear functions in the xy plane with the same y-intercepts and x-coefficients that are associated with the bounding planes. The top and bottoms lines are expressed as

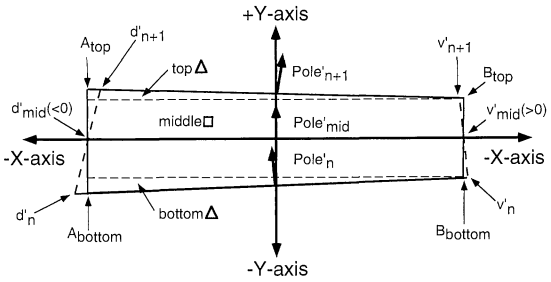

FIGURE 7. Sagittal plan view of the geometry of a hypothetical subslab that has been rotated and translated to the origin. The points A_{bottom}, A_{top}, B_{bottom}, and B_{top} are used to approximate the sagittal area of the subslab. See Center of Mass Calculation section in the text for the derivations of the labeled regions.

$$l_{top}(x) = c_{top} + a_{top} \cdot x \; l_{bottom}(x) = c_{bottom} + a_{bottom} \cdot x \tag{12}$$

where c_{top}, a_{top}, c_{bottom}, and a_{bottom} are the coefficients from the equations defining the top and bottom bounding slices of the current subslice. The lefthand limits, A_{top} and A_{bottom}, and the righthand limits, B_{top} and B_{bottom}, of the top and bottom triangles are computed using the l_{top} and l_{bottom} functions:

$$A_{top} = l_{top}(d\_mid_x) \qquad B_{top} = l_{top}(v\_mid_x) \tag{13}$$

$$A_{bottom} = l_{bottom}(d\_mid_x) \qquad B_{bottom} = l_{bottom}(v\_mid_x). \tag{14}$$

These limits are used to compute the areas of the top and bottom triangles and the middle rectangle:

$$area_{top\Delta} = \frac{1}{2}(v\_mid_x - d\_mid_x) \times |B_{top} - A_{top}| \tag{15}$$

$$area_{bottom\Delta} = \frac{1}{2}(v\_mid_x - d\_mid_x) \times |B_{bottom} - A_{bottom}| \tag{16}$$

$$area_{\text{rectangle}} = (v\_mid_x - d\_mid_x) \times (\min(A_{top}, B_{top}) - \max(A_{bottom}, B_{bottom})) \tag{17}$$

where "min" and "max" in the rectangle area expression are functions that return the minimum and maximum of a pair of numbers supplied to them.

To compute the Cd of a triangular region two integrations are required—one for the x-coordinate and one for the y-coordinate. Using the top triangle as an example, the x-position of the top triangle Cd is given by

$$Cd^{x}_{top\Delta} = \frac{1}{area_{top\Delta}} \times \int_{x=d\_mid_x}^{v\_mid_x} x \cdot \{l_{top}(x) - \min(A_{top}, B_{top})\}\, dx. \tag{18}$$

The y-position uses one of two expressions depending on which way the bounding lines limit points is the largest. If B_{top} is larger than A_{top} then the y-position of the triangle Cd is given by

$$Cd^{y}_{top\Delta} = \frac{1}{area_{top\Delta}} \times \int_{y=A_{top}}^{B_{top}} y \cdot \left\{ v\_mid_x - \frac{y - c_n}{a_n} \right\} dy. \tag{19}$$

If A_{top} is larger than B_{top} then the y-position is given by

$$Cd^{y}_{top\Delta} = \frac{1}{area_{top\Delta}} \times \int_{y=B_{top}}^{A_{top}} y \cdot \left\{ \frac{y - c_n}{a_n} - d\_mid_x \right\} dy. \tag{20}$$

A similar set of integrations is done to estimate the Cd of the bottom triangle. The Cd of the middle rectangle, because of the way the midslice was defined and then translated to the origin, will lie at the origin so no extra computations are needed.

To find the Cd of the whole quadrilateral region it is necessary to determine how the Cds of the two triangles displace the Cd of the middle rectangle. The x- and y-positions of the quadrilateral Cd are given by

$$Cd\begin{bmatrix}x\\y\end{bmatrix}'_{quad} = \frac{area_{top\Delta}\cdot Cd\begin{bmatrix}x\\y\end{bmatrix}_{top\Delta} + area_{bottom\Delta}\cdot Cd\begin{bmatrix}x\\y\end{bmatrix}_{bottom\Delta}}{area_{top\Delta} + area_{\text{rectangle}} + area_{bottom\Delta}}. \quad (21)$$

Cd'_{quad} is the pair of numbers representing the centroid of the rotated and translated subslice. To get the correct (original) position for the centroid the two numbers need to be adjusted to undo the effects of rotation and translation. This correction is done by the following matrix expression:

$$Cd\begin{bmatrix}x\\y\end{bmatrix}_{quad} = \begin{bmatrix}\cos(-\phi) & -\sin(-\phi)\\ \sin(-\phi) & \cos(-\phi)\end{bmatrix}\cdot Cd\begin{bmatrix}x\\y\end{bmatrix}'_{quad} + \begin{bmatrix}c_x\\c_y\end{bmatrix}_{mid} \quad (22)$$

where ϕ is the the angle by which the pole to the midplane was originally rotated by, and c_x and c_y are the original coordinates of the center of the associated midslice prior to translation.

The moments of the m^{th} slab with respect to the x- and y-axes are simply the sums of the moments of the subslabs:

$$slab\_mom\begin{bmatrix}x\\y\end{bmatrix}_m = \sum_{n=0}^{N-1} subslab\_volume_n\cdot\left(Cd\begin{bmatrix}x\\y\end{bmatrix}_{quad}\right)_n. \quad (23)$$

The CM of the entire body (in the sagittal plane) is determined by dividing the sum of the moments of all the body slabs by the the sum of the masses of all the slabs:

$$body\_CM\begin{bmatrix}x\\y\end{bmatrix} = \frac{\sum_{m=0}^{M-1} slab\_mom\begin{bmatrix}x\\y\end{bmatrix}_m}{\sum_{m=0}^{M-1} slab\_mass_m} \quad (24)$$

where M is the number of slices used to define the body volume. The masses of the slabs are equivalent to the slab volumes mulitiplied by some density.

A set of calculations, identical to those outlined above, are also applied to the slice data for lungs and other body cavities. The CMs for the body and any cavities can be combined to give a CM for the body + cavity(cavities). As a simple example, the CM of a body + lung arrangement would be expressed as

$$\frac{body\_CM\begin{bmatrix}x\\y\end{bmatrix}\cdot body\_mass + lung\_CM\begin{bmatrix}x\\y\end{bmatrix}\cdot lung\_mass}{body\_mass + lung\_mass} \quad (25)$$

In all these expressions for CM the z-term has been left out, and is assumed to be zero. The terms *body_mass* and *lung_mass* are just the volumes multiplied by some density. For the *lung_mass* the density will be less than the body density because it is mostly empty space.

Accuracy of Volume Estimates.—The accuracy of estimating a volume by slicing was tested by computing the volume of a triaxial ellipsoid with increasing numbers of slabs and increasing numbers of perimeter points to define the slabs. The slab count ranged from 2 to 32, while the number of points per slice varied from 4 to 32. Figure 8 shows the rapid improvement in the visual appearance of the ellipsoid as the numbers of slabs and points is increased. Table 1 shows the equally rapid improvement of the volume estimates with increasing numbers of slabs and points. The accuracy of the volume estimate, the fraction of the actual ellipsoid volume that the estimate represents was expressed as

$$100\cdot\frac{volume_{(m,n)}}{(4\pi/3)abc} \quad (26)$$

where $volume_{(m,n)}$ is the ellipsoid volume estimated with m slabs and n points per slab, and $(4\pi/3)abc$ is the exact volume of a triaxial ellipsoid with three different radii a, b, and c. The region on the top right of Table 1 represents volume estimates that are equal to 96.3%, or more, of the true volume of the ellipsoid. This flat region is reached when 16 slabs defined by 16 points are used to estimate the volume. The shape defined by 16 slabs and 16 points is also a good visual approximation of a triaxial ellipsoid. Increasing the number of slices or points beyond 16 gives only minor

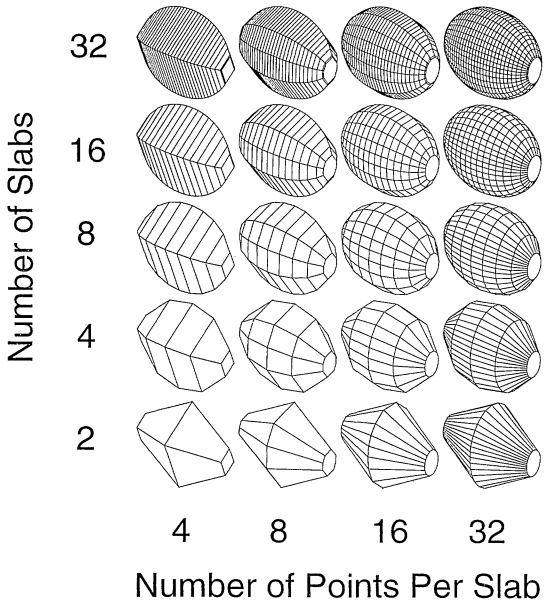

FIGURE 8. Graphical illustration of the improving visual representation of a triaxial ellipsoid when increasing numbers of slabs (slices) and points are used to define the ellipsoid. Lengths of the three radii of the ellipsoid are a = 1, b = 1.6, c = 2.4. The volume estimates associated with each ellipsoid are presented in Table 1.

TABLE 1. Improving estimates for the volume of a triaxial ellipsoid with increasing numbers of slabs and/or numbers of points per slab. Estimates are expressed as percentages of the true volume.

	Fraction of true volume (%)			
No. of slabs				
32	63.3	89.0	96.7	98.8
16	63.0	88.6	96.3	98.4
8	61.9	87.1	94.7	96.6
4	57.6	81.0	88.1	89.9
2	42.6	59.8	65.0	66.4
No. of points per slab	4	8	16	32

improvements in the accuracy of the volume estimate and appearance of the elllipsoid. Inspection of Table 1 shows that the volume estimates improve slightly faster with increasing numbers of points than with increasing numbers of slabs. This example gives an idea of how many slices would be needed to get a satisfactory quantitative and visual representation of a body form.

Body Length Estimates.—The lengths of the body models were determined by summing the distances between the center points of adjacent slabs. To make the comparisons of dinosaur body mass estimates from different studies simpler it was felt that estimates of body lengths for all the dinosaurs should be quoted along with all the mass estimates. Length estimates for the animals studied by Alexander were made from the drawings of Alexander (1985: Fig. 1). The straight-line distance from the tip of the snout to the tip of the tail of each animal was multiplied by the scale factor associated with each drawing. Colbert (1962) did not provide the total body lengths of his models. He did, however, supply model and actual hip heights. Estimates of the life sizes of the taxa used by Colbert were made with the following two assumptions: that the models used by Alexander and Colbert were of roughly the same shape and posture, and that the skeletal hip height quoted by Colbert was measured from the sole of the hind foot to the crest of the ilium. A similar hip height was estimated from Figure 1 of Alexander (1985), and a simple ratio expression was used to estimate the body lengths associated with the Colbert weight data:

$$total\_length_{Colbert} = \frac{total\_length_{Alexander}}{hip\_height_{Alexander}} \cdot hip\_height_{Colbert}. \quad (27)$$

Materials

Living Taxa

To test the predictions of the computational methods presented in this paper four large, living animals were chosen as test subjects: an elephant (*Loxodonta a. africana*), a giraffe (*Giraffa camelopardalis*), a hippopotamus (*Hippopotamus amphibius*), and a rhinoceros (*Ceratotherium simum*). The body forms and dimensions were taken from the illustrations in Kingdon (1997). The body density used for these four mammals was 1000 kg/m^3. The same density was also used for the horns of the rhinoceros, but the density of the elephant tusks was set to that of dentine (2000 kg/m^3) (Behrensmeyer 1990).

Extinct Taxa

The five genera used by Alexander (1985)—*Tyrannosaurus, Stegosaurus, Iguandon, Diplodocus,* and *Triceratops*—were also used in the

present study, the only difference being the use of more recent reconstructions for the body shapes and postures. A uniform body density of 1000 kg/m^3 was used to convert the dinosaur volume estimates to mass estimates. This value was chosen partly to simplify comparisons of body mass with those of Alexander, and because it required the fewest assumptions about the variation of density within the bodies of the animals.

Two forms of *Tyrannosaurus rex* were modeled. One, with a very rotund thoracic area, was taken from the reconstruction by Paul (1988: p. 341). It was felt that the chest area of this *Tyrannosaurus* may be too bulky, so a second, more slender form was also generated. The only modifications made to produce this slimmer one were reductions of the transverse widths in the chest area. This slimmer form corresponds, in part, with the *Tyrannosaurus* model of Farlow et al. (1995), which also has a narrower chest.

The reconstructed stegosaur is *Stegosaurus stenops* and was taken from Paul (1987: Fig. 19), which provided lateral, dorsal, and anterior views. The caudal spines were not used in any of the body mass and moment calculations, but the masses of the dorsal plates were used in the estimation of the body mass. The dimensions of the plates used are those displayed in the figure, the thickness of the plates was set to a constant 15 cm for all the plates, and a density of 1000 kg/m^3 was assumed.

The reconstruction of *Iguanodon bernisartensis* was based on the skeletal reconstruction from Norman and Weishampel (1990: Fig. 25.22). The dimensions in the frontal plane were based partly on the anterior views of *Iguanodon* in a painting by Douglas Henderson (in Czerkas and Olsen 1987, Vol. I: p. 9), and partly on views of hadrosaurs such as that of Paul (1987: Fig. 25).

The body form of *Diplodocus* is from a lateral view reconstruction of McIntosh et al. (1997: Fig. 20:11). The tranverse dimensions of this animal model were based on consultations with Paul Upchurch (personal communication 1997).

The sagittal profile of *Triceratops* was taken from Dodson (1996: Fig. 3.7b), while a dorsal view from Bakker (1987: Fig. 19) supplied the frontal plane dimensions. The masses of the brow horns and the parieto-squamosal frill were used in the computations of the total body mass. The frill thickness was set to a constant 5 cm and a density of 1700 kg/m^3 (Behrensmeyer 1990) was used for both the frill and horn mass estimates.

In estimating the widths of the intergirdle region of the herbivorous forms, it was assumed that these animals would be quite bulky due to the presence of the large digestive tracts needed to process large quantities of low-grade fodder (Farlow 1990). For the widths of the neck region the herbivores were given more slender necks, except for the neck of *Triceratops* and the base of the neck of *Diplodocus*. The neck width of *Tyrannosaurus* was kept large in light of the probable feeding style of these animals—the head being pulled back with the jaws clamped firmly onto the prey, which would have required powerful neck muscles.

The lung volumes used in the computations were produced by reducing the lateral and vertical dimensions of the body outline in the thoracic area until the computed lung volume was equal to 10% (±0.5%) of the total body volume. This value of 10% was chosen for consistency with the assumed lung volume used by Alexander (1985). The anterior extent of the lungs was set to lie between, or slightly anterior to, the shoulder girdles. The posterior extent of the lungs was adjusted to correspond to the approximate position of the posteriormost rib.

→

FIGURE 9. Illustrations of the body forms of four extant, large animals used to test the mass estimates computed by the method outlined in the text. Actual and estimated weights are presented in Table 3. A, Hippopotamus (*Hippopotamus amphibius*). B, African elephant (*Loxodonta a. africana*). C, Grass (White) Rhinoceros (*Ceratotherium simum*). D, Giraffe (*Giraffa camelopardalis*). Scale bar in all figures is 1 m with 20-cm divisions. Body shapes and dimensions are from Kingdon (1997).

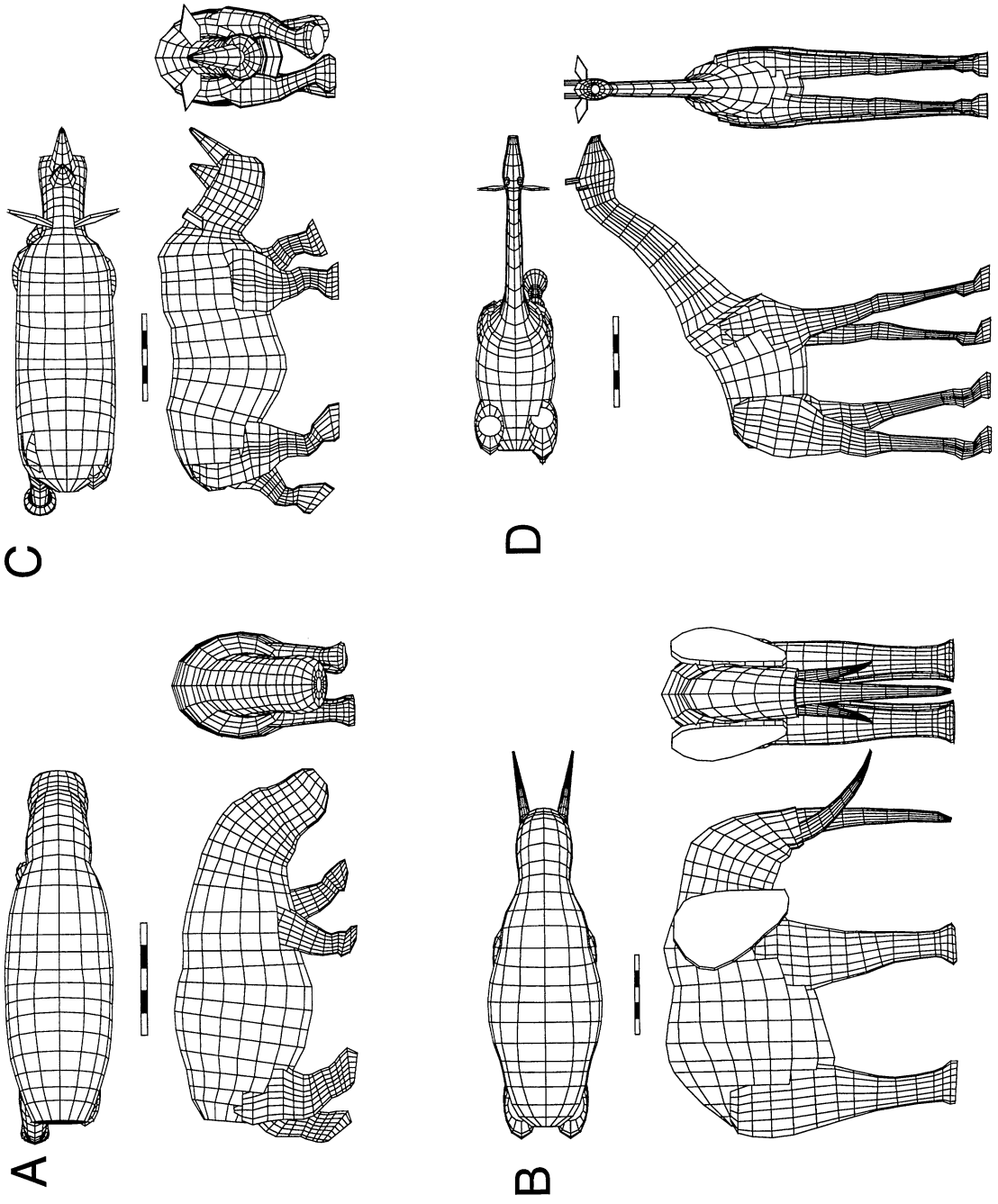
A
B
C
D

TABLE 2. Computed estimates of body element masses and total body masses for the mammal body forms shown in Figure 9. All masses are in kilograms.

Taxon	Head + body mass	Leg mass	Arm mass	Extra masses	Total mass	Total mass less 10% for lung cavity
Elephant	4922	532	484	172*	7126	6413
Giraffe	638	79	185	–	1166	1049
Hippopotamus	1706	79	48	–	1960	1764
Rhinoceros	2704	203	203	25**	3541	3187

* Elephant extras: 2 tusks = 50 kg each + trunk = 72 kg.
** Rhinoceros extras: 2 nose horns of 8 kg and 17 kg.

Results

Living Taxa

Figure 9 presents orthogonal views of the four living, large animals that were used as tests cases for the method presented here. The components of the mass estimates—masses of the head and body, legs, arms, and any extras—were all computed using the same method implemented in the same program, and these mass estimates are all presented in Table 2.

Comparisons of the predicted masses with the actual masses of the living animals are presented in Table 3. The model and real results are very close. The giraffe and rhinoceros model estimates differ by 11% from the values listed for the living animals, the largest differences of the four estimates, but the mass estimates of the living forms are quite variable. The estimated total body masses for the living animals supplied by Kingdon (1997) range from 450 kg to 1180 kg for female giraffes with a head height of 3.5–4.7 m, and from 2000 kg to 3600 kg for rhinoceri with shoulder heights of 1.7–1.85 m.

Extinct Taxa

Figure 10 presents the body and lung surfaces and the positions of the centers of mass for the five genera of dinosaurs. Table 4 lists the mass estimates of body components used to arrive at the final estimates for total body mass, and Table 5 compares the results of this study with those of Alexander (1985) and Colbert (1962).

Using the more recent dinosaur reconstructions, the mass estimates for the animals either range between the Alexander and Colbert estimates or are less than them. This pattern holds even when the length, and associated mass, of the stegosaur used by Alexander is scaled up to match that of stegosaur of the present study:

$$2825 \text{ kg} = 2000 \text{ kg} * (5.61 \text{ m}/5 \text{ m})^3 \quad (28)$$

where 2825 is the estimated body mass of the model used by Alexander if its length was 5.61 m, 2000 kg is Alexander's 1985 estimate for the body mass of *Stegosaurus*, 5 m is the length of his model animal, and 5.61 m is the length of the *Stegosaurus* used in the present study. This scaling relationship makes use of the fact that

TABLE 3. Comparisons of computed mass estimates and observed mass for living examples of the taxa in Figure 9. Observed animal dimensions and masses from Kingdon (1997) except for hippopotamus. All lengths are in meters and masses in kilograms.

	Model dimensions and masses			Observed dimensions and masses		
Taxon	Head + body length	Shoulder height	Total mass	Head + body length	Shoulder height	Total mass
Elephant	3.6	3.6	6413	4.0	4.0	6300
Giraffe	3.5	4.5*	1049	3.7	4.7*	1180
Hippopotamus	3.2	1.55	1764	3.2**	1.55**	1618**
Rhinoceros	3.8	2.0	3187	3.5	1.85	3600

* Height of giraffe head above ground.
** Scaled weight estimate for an animal that is geometrically similar to a hippopotamus of length = 4.5 m and weight = 4500 kg (Hildebrand 1982: p. 428).

TABLE 4. Computed estimates of body element masses and total body masses for the dinosaur body forms shown in Figure 10. All masses are in kilograms.

Taxon	Head + body mass	Leg mass	Arm mass	Extra masses	Total mass	Total mass less lung cavity
Tyrannosaurus	6081	896	–	–	7873	7224
Stegosaurus	1722	295	53	393*	2811	2530
Iguanodon	2657	523	187	–	4077	3790
Diplodocus	13,040	729	207	–	14,912	13,421
Triceratops	3528	294	88	83**	4375	3938

* *Stegosaurus* extras: 12 dorsal plates.
** *Triceratops* extras: 2 brow horns = 13 kg each + frill = 57 kg.

the change in mass is proportional to the cube of the change in the linear dimension. This scaling assumes that the two models are geometrically similar.

The relatively small values for the estimated masses of the dorsal plates of *Stegosaurus*, 393 kg, and the parietal-squamosal frill and brow horns of the *Triceratops*, 83 kg, will have little effect on the final result of the masses of the animals. The masses of these extra bony elements are minor fractions of the total body mass. The effects of including the plates of the *Stegosaurus*, or the frill and horns of the *Triceratops*, would have had only minor effects on the final results of the CM for these animals.

As argued semiquanitatively by Alexander (1985), the inclusion of the lungs in estimates of the CM has only a minor effect of the final position of the CM. The magnitudes of the shift in position of the CM when a lung cavity is included in the analysis of body mass distribution are shown in Table 6.

The difference between the positions of the CM for the "thick" *Tyrannosaurus* and the "thin" one is also relatively minor—just over half of one percent of the total body length (0.06 m/10.7 m). The wider chest of the "thick" *Tyrannosaurus* gives this model an extra 684 kg of mass around the anterior portion of the trunk. This added mass is approximately equal to 10% of the total body mass of the "thin" *Tyrannosaurus*, almost equal to the mass excluded to make space for the lung cavity. The shift in the position of the CM in these two cases of changing mass, lung volume subtraction, and chest mass addition are also roughly equal. Dorsal and lateral views of this shift in CM position are presented in Figure 11.

Discussion

The assumption of a uniform density for the models will have the greatest effect on the mass and CM of the sauropod. The extensively modified cervical vertebrae and small head of these animals suggest that minimization of the mass projected forward from the shoulder girdle was of paramount importance. Undoubtedly the bulk density of the neck region was less than 1000 kg/m^3. This reduction of the neck density would have the effect of shifting the CM posteriorly, making the possibility that sauropods were able to rise up onto their hind legs more likely (Bakker 1987). The method outlined in this paper would allow for the inclusion of multiple cavities that may have

TABLE 5. Comparison of various body mass estimates for large dinosaurs. Total body lengths quoted for the models in this study are the sums of the center-to-center distances between transverse slices for a given model. Lengths are in meters and masses are in kilograms.

	This study		Alexander 1985		Colbert 1962	
	Total body length	Body mass	Total body length	Body mass	Total body length	Body mass
Tyrannosaurus	10.7	7224	10.7	7400	10.9	6890
*Tyrannosaurus**	10.7	7908				
Stegosaurus	5.61	2530	5.0	2000	5.3	1780
Iguanodon	7.85	3790	8.1	5400	7.7	4510
Diplodocus	22.4	13,421	20.3	18,500	18.0	10,560
Triceratops	6.22	3938	7.8	6100	5.5	8480

* *Tyrannosaurus* with wider chest area from Paul (1988: p. 341).

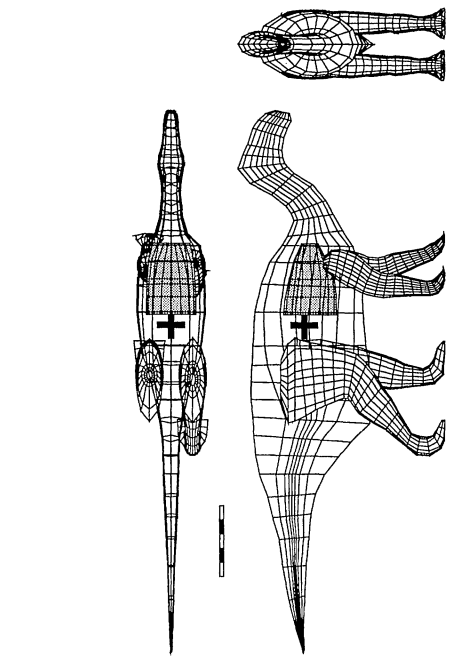
C

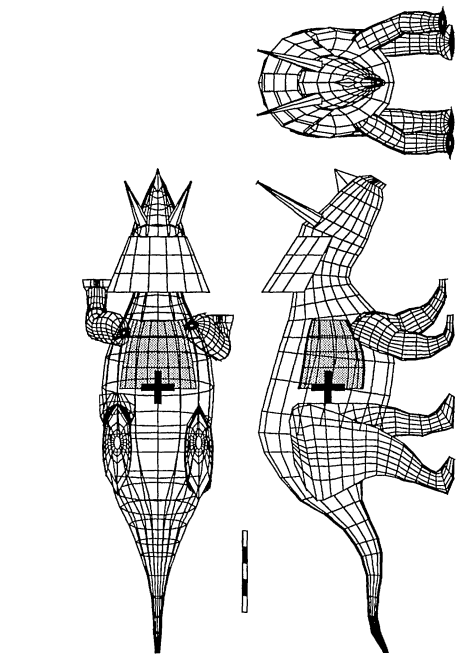
D

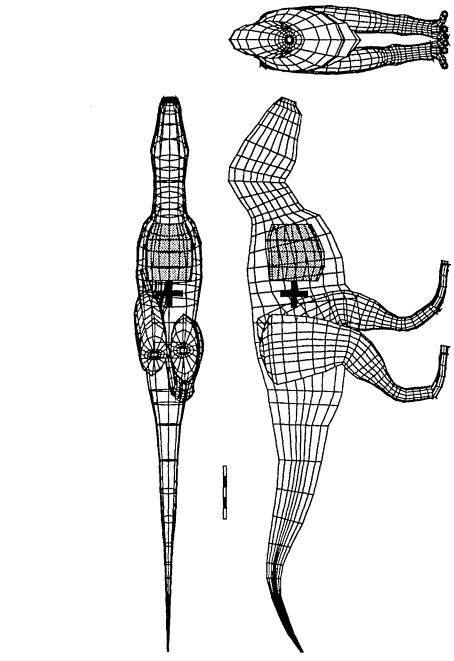
A

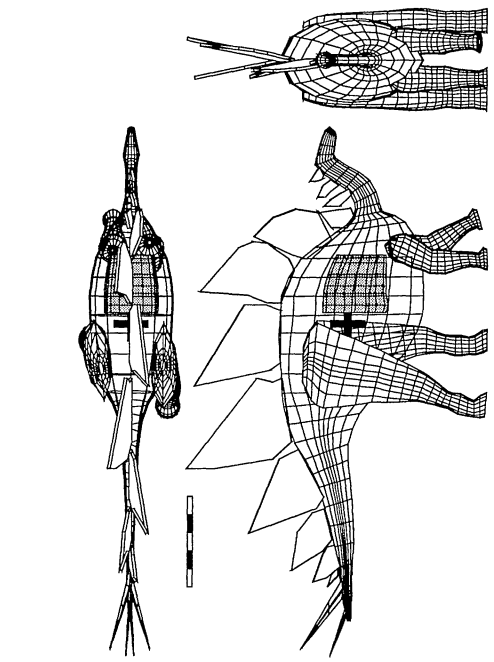
B

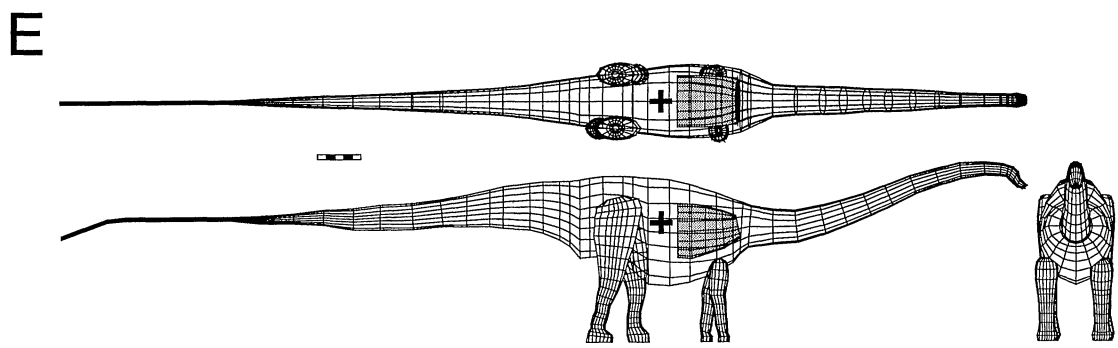

FIGURE 10. Dorsal, lateral, and anterior views of dinosaur body forms, lung cavities, and associated centers of mass. A, *Tyrannosaurus rex,* slender form (modified from Paul 1988). B, *Stegosaurus stenops* (from Paul 1987). C, *Iguanodon bernisartensis* (from Norman and Weishampel 1990). D, *Triceratops horridus* (from Dodson 1996). E, *Diplodocus* (from McIntosh et al. 1997). Gray cylinders in anterior trunk regions are the hypothetical lung volumes associated with each model. The center of mass of the lung + body is shown by the large black cross. Scale bars in all figures are 1 m with scale increments of 20 cm.

occupied the pleurocoels of the cervical and dorsal vertebrae of sauropods. This approach was not tried in this study in order to maintain consistency with earlier estimates of mass and centers of mass.

The effects of changes in mass of models of up to 10% were examined by subtracting mass to approximate the presence of a lung cavity, and increasing the width of the chest area of the *Tyrannosaurus.* In all cases the magnitudes of the shift in CM due to the mass changes were relatively small. It appears that a reconstructed body form would have to have a substantially different shape to have a significant effect on the position of the CM. In contrast, a change in the linear dimensions of a model will have a significant effect on the body mass estimate because of the cubic relationship between linear dimension and mass.

The masses of the legs and arms were not included in the computations of CM. The view was taken that limbs are functionally distinct from the axial body (head, neck, trunk, and tail). Large quadrupedal dinosaurs, with the possible exception of diplodocid sauropods, would have rarely lifted the anterior part of the body off the substrate. The only truly bipedal dinosaur of this study, *Tyrannosaurus rex,* has such small forelimbs that the added mass that they represent can be safely ignored. The CMs experienced relatively small changes in position due to the subtraction of the lung cavity from the anterior part of the trunk. The effect of adding the weight of the forelimbs in a semibipedal form like *Iguanodon* would have had a similarly minor effect on the CM.

A serious hazard in estimating the masses of large animals from scale models is the sensitivity of the final mass estimate to the effects of small errors in the dimensions of the model. Colbert (1962) and Farlow et al. (1995) also commented on the need for very accurate modeling. Multiplying a dimension, incor-

TABLE 6. Positions of the centers of mass (CM) of body, lung, and body + lung in the sagittal plane (Z = 0). x = values measured horizontally from the tip of the tail. y = values measured vertically from the soles of the feet. Last column shows the displacement of the Body CM when the lungs are included. All units are in meters.

	Body		Lung		Body + lung		Displacement	
	x_B	y_B	x_L	y_L	x_{BL}	y_{BL}	$x_{BL} - x_B$	$y_{BL} - y_B$
Tyrannosaurus	6.68	2.86	7.50	2.86	6.76	2.86	0.08	0.0
*Tryannosaurus**	6.77	2.87	7.50	2.86	6.82	2.87	0.05	0.0
Stegosaurus	3.33	1.51	3.7	1.42	3.36	1.50	0.03	−0.1
Iguanodon	4.59	1.91	5.16	1.87	4.65	1.91	0.06	0.0
Diplodocus	13.7	2.77	14.8	2.6	13.8	2.75	0.10	−0.2
Triceratops	3.25	1.49	3.63	1.47	3.28	1.49	0.03	0.0

* After Paul 1988.

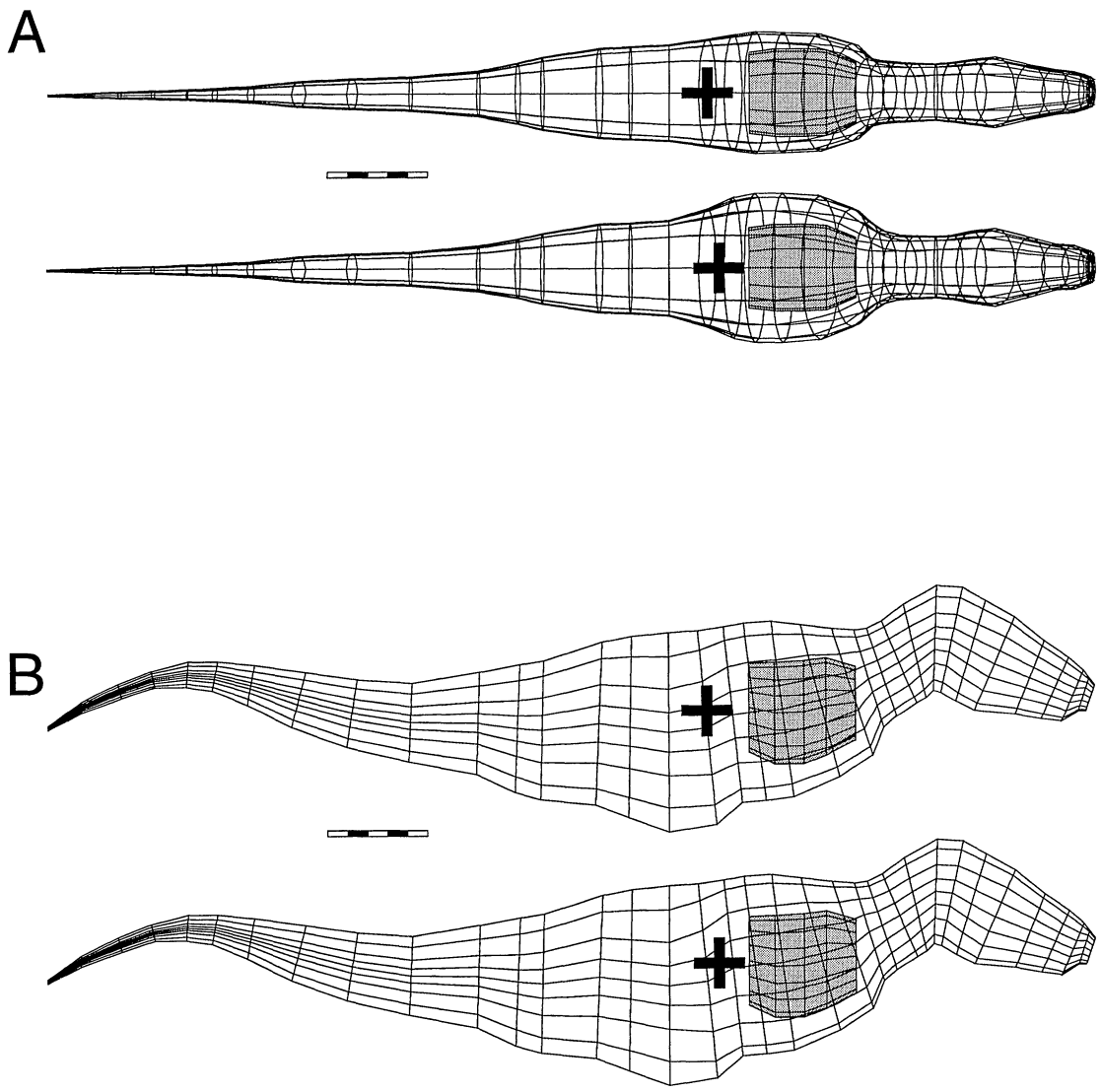

FIGURE 11. Dorsal (A) and lateral (B) views of the two tyrannosaur body forms that were "weighed" and "centered" in this study. The upper body form in both images is similar to that of Farlow et al. (1995), while the lower body form image, with the wider thoracic region, is based on the reconstruction of Paul (1988). The slight difference in the positions of the center of mass of the "thick" and "thin" body forms is visible as a modest antero-dorsal displacement of the black cross in the thick form relative to that in the thin one. Quantitative results for this comparison are presented in Table 6. Scale bars in both figures are 1 m with 20-cm divisions.

rectly measured from a tracing, by a scaling factor will magnify the error. This error gets compounded if the dimension is squared when calculating an area, or cubed to calculate a volume. For the method outlined here there are two situations where small errors in data collection will lead to large variations in the mass estimates.

The first error would arise during the generation of the body outlines. A slightly wider or deeper neck will add mass to the front of the animal. This extra mass will shift the CM anteriorly. A similar, but opposite, effect will occur if the dimensions of the tail are too large. The addition of too many caudal or cervical vertebrae will also shift the CM backward or forward from its true position. This is most problematic when estimating the CM of

the larger sauropods, where a small mass, positioned far from the main body mass, can have a strong effect on the longitudinal position of the CM.

The second error would arise when the x, y, and z coordinates are being collected. Careless positioning of a digitizing stylus, or poor visual estimation of grid coordinate values that lie between marked grid lines on graph paper, will produce errors in dimensions. Once the measurements were entered into the computer, it was found that plotting the raw profile data by a graphics program often allowed for the visual detection of sloppy data collection. The breaking of left-right symmetry was also very apparent when frontal profiles were plotted, and this allowed for the rapid identification of errors in measurement.

A final source of error is due to the present method overestimating the amount of mass in the pelvic region ventral to the acetabulum of the saurischian dinosaurs—*Tyrannosaurus* and the *Diplodocus*. The ventral dimensions of the slices in this region are defined by the edges of the ventralmost margins of the pubis and ischium. While there would have been prominent muscles originating from the proximal regions of the pubis (e.g., pubo-ischio-femoralis externus) and ischium (e.g., adductors and pubo-ischio-femoralis internus 3) (Romer 1923), presumably there was merely a sheet of skin spanning the distal portions of the arc between the ventral edges of the pubis and ischium. To keep the computations of body volume simple it was assumed that body tissues in this region filled the full area of the elliptical slice. This overestimate of mass ventral to the acetabulum is probably partly compensated for by an underestimate of the mass dorsolateral to the acetabular rim and iliac crest. Large muscles such as the ilio-femoralis and ilio-fibularis were not explicitly included in the definitions of the body contours. Fortunately, the proximity of pelvic region to the CM ensures that the moment arms associated with any deficits or excesses of mass are small enough to not have a significant effect on the final position of the CM. The good agreement between the CM positions of this study and those of Alexander (1985) indicates that this source of error is not significant.

Conclusions

A numerical/computational method for the collection of body form data and the determination of body mass parameters, as outlined in this paper, makes it relatively easy to study the dynamics of a vertebrate body. With the body data in electronic form, the testing of hypotheses concerning the biomechanics of both extinct and extant animals can be done quickly and more easily. Volume-based mass estimates can allow testing of body mass estimates made by other means such as the long-bone dimension method of Anderson et al. (1985).

The software used to convert digitized data from computer-aided drafting (CAD) packages and paint programs such as CANVAS into simple data files, to transform 2-D slice data into 3-D meshes, and to compute volumes and centers of mass of meshes is available free of charge. For instructions on obtaining and using this software contact the author.

Acknowledgments

I thank M. Benton and G. Helffrich, both of the Department of Earth Sciences, University of Bristol, for early reviews, constructive criticisms, and advice on the presentation of the images. Many thanks to I. Stewart of Computing Services, University of Bristol, for help on technical matters related to PV-WAVE programming and the generation of 3-D images. The comments and suggestions of the two reviewers, S. C. Bennett and M. Carrano, greatly improved the finished manuscript.

Literature Cited

Alexander, R. McN. 1983. Animal mechanics, 2d ed. Oxford University Press, Oxford.

———. 1985. Mechanics of posture and gait of some large dinosaurs. Zoological Journal of the Linnean Society 83:1–25.

Anderson, J. F., A. Hall-Martin, and D. A. Russell. 1985. Long-bone circumference and weight in mammals, birds, and dinosaurs. Journal of Zoology 207:53–61.

Bakker, R. T. 1987. The return of the dancing dinosaurs. Pp. 39–69 *in* S. J. Czerkas and E. C. Olsen, eds. Dinosaurs past and present I. Natural History Museum of Los Angeles County, Los Angeles.

Behrensmeyer, A. K. 1990. Bones. Pp. 232–235 *in* D. E. G. Briggs and P. R. Crowther, eds. Paleobiology: a synthesis. Blackwell Scientific, Oxford.

Bramwell, C. D., and G. R. Whitfield. 1974. Biomechanics of *Pteranodon*. Philosophical Transactions of the Royal Society of London B 267:503–581.

Colbert, E. C. 1962. The weights of dinosaurs. American Museum Novitates 2076:1–16.

Czerkas, S. J., and E. C. Olsen, eds. 1987. Dinosaurs past and present I and II. Natural History Museum of Los Angeles County, Los Angeles.

Damuth, J., and B. J. MacFadden, eds. 1990. Body size in mammalian paleobiology: estimation and biological implications. Cambridge University Press, Cambridge.

Dodson, P. 1996. The horned dinosaurs. Princeton University Press, Princeton, N.J.

Farlow, J. O. 1990. Speculations about the diet and digestive physiology of herbivorous dinosaurs. Paleobiology 13:60–72.

Farlow, J. O., M. B. Smith, and J. M. Robinson. 1995. Body mass, bone "strength indicator", and cursorial potential of *Tyrannosaurus rex*. Journal of Vertebrate Paleontology 15:713–725.

Gatesy, S. M., and A. A. Biewener. 1991. Bipedal locomotion: effects of speed, size and limb posture in birds and humans. Journal of Zoology 224:127–147.

Gregory, W. K. 1905. The weight of the *Brontosaurus*. Science, new series 22(566):572.

Hildebrand, M. 1982. Analysis of vertebrate structure, 2d ed. Wiley, New York.

Kingdon, J. 1997. The Kingdon field guide to African mammals. Academic Press, London.

McIntosh, J. S., M. K. Brett-Surman, and J. O. Farlow. 1997. Sauropods. Pp. 264–290 *in* J. O. Farlow and M. K. Brett-Surman, eds. The complete dinosaur. Indiana University Press, Bloomington.

Norman, D. B., and D. B. Weishampel. 1990. Iguanodontidae and related ornithopods. Pp. 510–533 *in* D. B. Weishampel, P. Dodson, and H. Osmólska, eds. The Dinosauria. University of California Press, Berkeley and Los Angeles.

O'Neil, P. V. 1983. Advanced engineering mathematics, 3d ed. Wadsworth, Belmont, Calif.

Paul, G. S. 1987. The science and art of restoring the life appearance of dinosaurs and their relatives. Pp. 4–49 *in* S. J. Czerkas and E. C. Olsen, eds. Dinosaurs past and present I. Natural History Museum of Los Angeles County, Los Angeles.

———. 1988. Predatory dinosaurs of the world. Simon and Schuster, New York.

Romer, A. S. 1923. The pelvic musculature of saurischian dinosaurs. Bulletin of the American Museum of Natural History 48:605–617.

Weishampel, D. B. 1995. Fossils, function, and phylogeny. Pp. 34–54 *in* J. Thomason, ed. Functional morphology in vertebrate paleontology. Cambridge University Press, Cambridge.